Return to EOS page

1997 Progress Report on EOS IDS

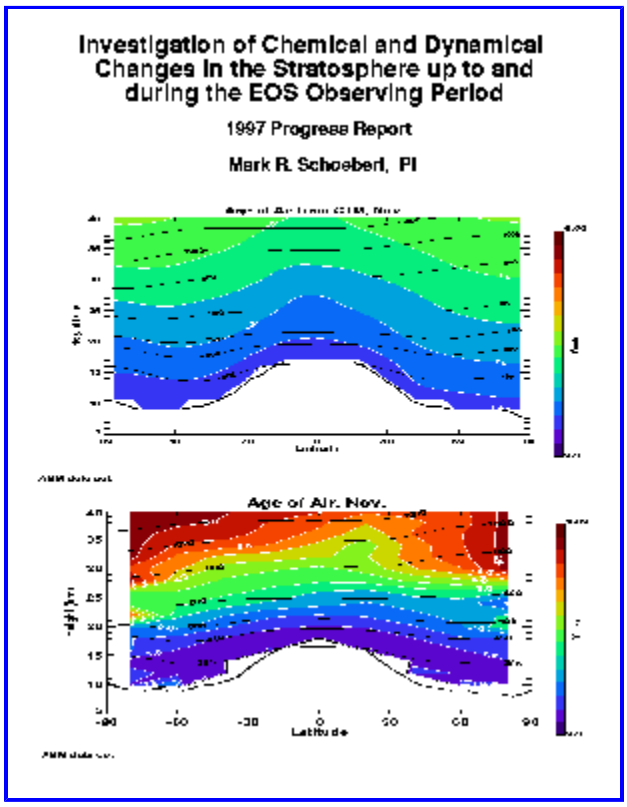

Investigation of Chemical and Dynamical Changes in the Stratosphere up to and During the EOS Observing Period

M. R. Schoeberl, P. I., *Goddard Space Flight Center*

Steve E. Cohn, *Goddard Space Flight Center*

Anne R. Douglass, *Goddard Space Flight Center*

James Gleason, *Goddard Space Flight Center*

Charles H. Jackman, *Goddard Space Flight Center*

Leslie R. Lait, *Hughes STX, Landover, MD*

Paul A. Newman, *Goddard Space Flight Center*

Richard B. Rood, *Goddard Space Flight Center*

Joan E. Rosenfield, *Goddard Space Flight Center*

Richard S. Stolarski, *Goddard Space Flight Center*

Anne M. Thompson, *Goddard Space Flight Center*

Marvin A. Geller, *State University of New York-Stony Brook*

Robert D. Hudson, *University of Maryland-College Park*

Summary

The activities under this IDS can be characterized as fitting into the categories of modeling or data analysis. On the modeling side, the chemical transport model (CTM) is being run in real time to support the Polaris mission. The CTM integrations are now showing very good agreement with the observations. As a science by product of this work, as discussed in Section 2.2, we are able to distinguish the recovery process in the northern hemisphere for two dynamically different years, 1993 and 1997. In 1992, there was a more or less normal break up of the north polar vortex, whereas in 1997, the vortex persisted into late April with significant ozone loss.

We have suspended our MODE experiments to reconfigure the model to work with Arctic data and to be initialized using the Chemical Transport Model (CTM). The CTM integrations are now good enough that we no longer need to rely on the UARS data for initialization

We are now doing age-of-air integrations with the trajectory model. Age-of-air appears to be a sensitive diagnostic of the dynamics and transport. Our comparisons with CTM age-of-air estimates suggest use of kinematic vertical velocities may be problematic as far as transport.

We continue to use both the fixed transport and the interactive 2D models to investigate ozone and climate changes. The dynamics was reformulated in the fixed 2D model along the lines of the interactive 2D model; the interactive 2D model now uses the chemical package of the fixed model. The fixed 2D model is able to simulate the global ozone changes observed by TOMS with excellent fidelity. The interactive model is being used to investigate the role of sub-visible cirrus formation in the tropics and its impact on the stratosphere. The interactive 2D model is also able to make a credible simulation of the HALOE water vapor observations.

We have also done a study to determine if small scale structures in ClO could significantly affect estimates of ozone loss. Using the observations from all the aircraft flights, we have been able to quantify the error in ozone loss due to small scales. Our computed ozone loss does not appear to be large, in contrast to the model studies by Edouard et al. [1996]. We continue to examining horizontal resolution issues using Reverse Domain Fill techniques and CRISTA data as surrogates for HIRDLS type measurements.

Major improvements in the DAO products are just starting to be generated. We have also pushed forward our efforts at constituent assimilation now focusing on column ozone using the forecast error technique developed by Riishojgaard, 1997.

Over the last year members of our IDS team have also served on NASA H committees reviewing the CHEM mission. Jim Gleason turned over his job as CHEM Project Scientist to P. K. Bhartia to focus on GOME data. GOME is a precursor instrument to SCIAMACHY which will be flown on ENVISAT.

This IDS team will be proposing to be part of the science team to propose utilizing ENVISAT data. Finally, this coming year we will be preparing for an EOS IDS reproposal.

Table of Contents

1.0 Background

1.1 Previous reports

Our 1996 report is located on the world-wide web at http://hyperion.gsfc.nasa.gov/EOS/report_1996/report.html. The 1995 report is located at http://hyperion.gsfc.nasa.gov/EOS/report_1995/report.html.

The introduction to the 1995 report summarizes our main research goals and progress up through 1995. This report stands as an update of the 1996 report. The sectional structure of this report is slightly different 1996 report.

1.2 Overview of Current Research Activities

Upper Atmosphere Research Satellite (UARS) data combined with aircraft mission data is the best prototype for the EOS CHEM instruments. Preparing for EOS CHEM data and chemical assimilation is the main focus of this investigation. Thus the tools this IDS has developed and our experience with UARS data is directly applicable to EOS program. A large part of our team is focused on the UARS data

set (Schoeberl, Douglass, Jackman, Rood, Geller, Newman, and Lait) as described below. Our group also has a large involvement in aircraft expeditions. Members of our IDS team participated in the AASE, AASE II, ASHOE/MAESA, TRACE A, STRAT, POLARIS, TOTE/VOTE, PEM Tropics, and SPADE aircraft missions and analysis of that data. We believe that aircraft and satellite data are complimentary and analysis of aircraft data is consistent with the interdisciplinary aspect of our proposal.

Model and data analysis tool development has been an important activity under this IDS. For example, an interactive 2D chemical model was developed under this IDS with new results discussed below. We have also participated in the 3D chemical modeling effort and have spun off a Lagrangian Chemical model which is being used to simulate ozone loss in the polar regions (see 1996 report). A lot of progress has been made on the stratospheric assimilation, and using trajectory models for age-of-air calculations as a diagnosis of the assimilation system.

In tropospheric chemistry we have focused mostly on development of better methods for satellite retrieval of tropospheric ozone as described below (Section 2.8).

In the 1999-2002 time frame, the ESA ENVISAT satellite is expected to be major source of new atmospheric trace constituent measurements. In particular the SCIMACHY instrument is expected to measure a significant number of these trace species. In preparation for SCIMACHY we have been analyzing the data from its predecessor instrument, GOME (Global Ozone Monitor) on the ERS-2 platform. The GOME instrument was a significant instrumental advance in that the instrument measures the complete backscattered spectrum from 240 to 800 nm. This new data set has lead to the development of new algorithms for the retrieval of atmospheric trace constituents. Specifically, we have been working with the GOME Team to adapt the NASA total ozone and ozone profile algorithms to the GOME radiance data, we can help separate instrumental from algorithimic artifacts in the retrieved products. We have helped the GOME Team identify algorithmic artifacts, such as how their total ozone values depend on the climatology used in their retrieval. We demonstrated that there were radiance jumps in their spectra that make ozone profile retrievals impossible without some type of spectral recalibration and adjustment. Future work will focus on the development of new data products that can be measured using the spectral information from GOME and SCIMACHY.

We have performed study on the impact of HIRDLS mapping as described below (Section 2.5). The trajectory automailer is also partially maintained under this IDS, the usage statistics are given in Section 6.

2.0 Science activities

2.1 Trajectory models

The trajectory chemical package is undergoing an upgrade as a result of the Polaris data. Thus our MODE (Multi-year ozone depletion experiment) has been suspended until this upgrade is finished. We are also intending to use the CTM to initialize the MODE experiments since the CTM results are quite reasonable and this overcomes our uncertainties associated with using the UARS data - not all needed species were measured by UARS. Thus we have suspended our work on MODE and shifted our effort to a project to compute age-of-air as described below.

2.1.1 Age-of-air calculations

Progress with the assimilation model is discussed below. We are now working on using age-of-air to diagnose the transport properties of the stratospheric assimilation model. The new technique uses long

term parcel trajectories computed using net diabatic heating rates. Figure 2.1.1-1 shows a snap shot during an integration. The parcels are colored by their age, and the background shows the net diabatic heating rate. The Lagrangian approach to age-of-air calculations is unique in that it produces a non-diffusive transport of material and is often superior to computations using standard Eulerian transport models.

The disadvantage of the Lagrangian approach is the rapid decrease of parcel numbers with altitude. Figure 2.1.1-2 shows the number of parcels verses altitude at the end of a 5 year integration. The -3.3 scale height means that the statistics of the parcels are uncertain above 30 km for the number of parcels used in this case study.

The age-of-air computations using the Goddard assimilation data (STRAT) and the UKMO data are shown in Figures 2.1.1-3a and 2.1.1-3b. The comparisons are fairly good. However, an age-of-air calculation using the CTM and the STRAT data set (Fig. 2.1.1-4) shows quite different results. The CTM has produced very young air at very high altitudes near the polar regions. This is inconsistent with the Lagrangian result. We believe that this result is due to use of the kinematic vertical velocity in the CTM which is far noisier than the diabatic vertical velocities used in the Lagrangian method. These results have important implication for the chemical models being run using the CTM. Another interesting result shown in Figs. 2.1.1-3 is how flat the distribution of ages is around the equator. This suggests that the assimilation winds (both STRAT and UKMO) winds are over mixing in the tropical region.

2.1.2 Aircraft Exhaust

Another application of the Lagrangian technique is analysis of aircraft exhaust dispersal. We have submitted a paper on this process to JGR [Schoeberl, et al., 1997]. An example of the results of this study are shown in Fig. 2.1.2-1 which shows snap shots of the evolution of a northern hemisphere air parcel release. The experiment shows the dispersal of parcels into both hemispheres and then into the troposphere. Our study concluded that aircraft exhaust released below the 380K surface in the stratosphere quickly leaves the stratosphere. Exhaust released above 380K has a lifetime of about one year. This result is in good agreement with the study of Weaver et al. [1996].

2.2 Stratospheric Chemical and Dynamical Modeling

This section describes some of the chemical and dynamical activities supported under this IDS. The testing and development of models as tools for our science objectives and analysis of EOS data is a critical activity in the pre-EOS time frame. Most of our activity centers around analysis of satellite and aircraft data sets .

2.2.1 Simulation of stratospheric constituents using the 3-D chemical model

The three-dimensional chemical model was developed under funding from the Atmospheric Chemistry Modeling and Analysis Program. The chemical package and transport scheme eventually will be used in the chemical assimilation effort. Thus, scientific testing of the 3-D CTM is essential for the success of the IDS assimilation program and also allows us to move toward our goal of using the 3-D chemical model for interpreting long-term trends.

There has been substantial progress in the 3-D chemistry and transport model in the last year. Full chemistry integrations of the model include ozone, reactive constituents important to the ozone evolution, and long lived source gases (Douglass et al., 1997). Because the winds and temperatures used

in this off-line simulation are taken from the GEOS-1 data assimilation system, the calculated constituent evolution is sensibly compared with observations. Simulations are complete for the following time periods: Nov. 15, 1991 - Sept. 1, 1992; Nov. 15, 1995 - April 22, 1996; March 18, 1997 - present.

The simulations are directed towards several goals. Both models and observations show interannual variability in lower stratospheric ozone loss in the northern hemisphere (e.g., Manney et al., 1994; Manney et al., 1996; Chipperfield et al., 1996). Simulations for 1991-92 and 1995-96 are being compared with observations to determine if the model is capable of correctly reproducing the interannual variability. In addition, the 95-96 simulation is being compared with VOTE/TOTE aircraft observations described below. Aircraft data was also collected during the Atmosphere-Ocean Chemistry Experiment (ACE) during April 1996. Flights were made through a midlatitude cut off low and observations of this event were presented by Moody et al. [1997]. Fields from the global simulation are being compared with these observations to determine if the model constituent distribution in the upper troposphere evolves realistically during this event, thus providing insight into the modeling of processes associated with stratosphere/troposphere exchange.

The current simulation which was begun March 18, 1997 is being run in near real time in support of the POLARIS mission. In addition, each day a five day forecast of the ozone field is calculated using the result of the full chemistry integration to initialize the forecast, the forecast winds from the DAO, and a parameterization for photochemical production and loss. In general the forecast fields for March 20, 1997 - May 18, 1997 compare well with observations from ADEOS TOMS data, although the quality of the comparison degrades after about a month of integration. Causes for the loss of forecasting skill are being considered currently.

Finally, the 1997 spring integration using the CTM is unique in that the northern polar vortex lasted much longer than in prior years since the launch of UARS. The ozone loss diagnosed from observations is high this year, and there are concomitant differences in the reformation of the chlorine reservoirs. The Halogen Occultation Experiment (HALOE) has observed HCl at high latitudes each northern spring since 1992. Comparison of the model fields with observations during the time period when heterogeneous reactions have ceased and the chlorine reservoirs are being reformed provides a test of model processes as the chlorine constituents exhibit transients which should be matched by the temporal evolution of modeled fields. Observations for 1992 and 1997 are compared with 3D model calculations in Figures 2.2.1-1 and 2.2.1-2 ; observations and model are normalized by dividing by the mixing ratio of total chlorine. For MLS ClO, MLS O3, and CLAES ClONO2 the time series shown in the figures are averages for the polar vortex. For late spring, the polar vortex remnant is identified by its low value of N2O. In the case of HALOE, the HALOE averages are for those profiles that are found within the polar vortex; the model averages at the time and location of the HALOE observations are given, as well as the model average within the polar vortex.

Comparisons of the model average over the vortex with the model average for the HALOE points provides an indication of how representative the HALOE average is of the entire vortex. For 1992, there is overall agreement in the time series for model ClOx, HCl, and ClONO2 with MLS ClO, HALOE HCl and CLAES ClONO2, noting that ClOx in the model includes the dimer Cl2O2 and thus it is not surprising that the model fraction exceeds the fraction of total chlorine which is seen as MLS (daytime) ClO. For 1997, (Fig. 2.2.1-2) the model integration does not begin until mid March. However, the ClO is elevated well into February (in contrast to 1992, Fig. 2.2.1-1), and the modeled and observed fractions of HCl and ClO are in good agreement in late March. During April, the modeled HCl rises rapidly, in good agreement with the observations. In late May, the modeled and observed fraction of Cly found in HCl is much larger than in 1992, and ClONO2 is correspondingly lower. Analysis of model and observations show that several factors contribute to the differences in temporal behavior of the chlorine

reservoirs, among them the ozone loss in 1997 which is much larger than in 1992. The good agreement of the model and observations under different meteorological conditions and for transient photochemical behavior is evidence that the photochemical and transport processes in the model interact appropriately on seasonal time scales, an important step towards using such model simulations in the interpretation of long term trends.

2.3 Chemical and Data assimilation

Part of this IDS investigation consists of providing timely feedback to the Goddard Data Assimilation Office (DAO) about remaining problems in the stratosphere Data Assimilation System (DAS). Response to this feedback generates improved stratospheric assimilations. User feedback is an important part of improving a DAS as users bring a wide range of experience, diagnostic tests, transport and trajectory models, and independent (unassimilated) observations. Improving the multi-year transport in the DAS is important for assessing potential climate change issues. This IDS investigation is continuing its close work with the DAO in its effort to improve the transport characteristics of the GEOS-2 DAS.

This past year has seen the development, testing, and validation of the GEOS-2 (Goddard Earth Observing System -2) Data Assimilation System (DAS). Many of the features in this new DAS have been specifically designed and tuned for improving stratospheric data assimilation in response to feedback provided by this IDS investigation. The GEOS-2 DAS is based on the new 70 level GEOS-2 GCM (General Circulation Model) coupled with the new Physical-Space Statistical Analysis System (PSAS). The GCM now includes an orographic gravity wave drag parameterization and Rayleigh friction tuned to eliminate the cold pole bias of the GEOS-1 GCM. The upper boundary of the GEOS-2 GCM is at 0.01 hPa (about 80 km), though the number of data analysis levels in the DAS remains at 18 with the top analysis level at 0.4 hPa (about 55 km).

One important feature of PSAS is the ability to adjust the horizontal correlation length at different altitudes so that observations can be distributed over larger horizontal areas in the stratosphere, corresponding to the larger scale of the dynamical variability in the stratosphere. The tuning of this horizontal scale coupled with a reduction in the vertical correlation scale has resulted in much smoother stratospheric potential vorticity fields than has been seen in previous assimilation produced winds and temperatures (Fig. 2.3-1). These smoother fields not only look more dynamical (advective) but, more importantly, they agree with the observations better than past assimilations. These improvements in the PV field may help reduce the lower stratospheric horizontal transport that in the past has been too rapid.

2.3.1 Chemical assimilation

In the 1996 EOS IDS report we have given an account of the development of a Kalman filter for stratospheric constituent assimilation of limb sounding observations (Lyster et al. 1997). Also shown was its potential in providing useful global field estimates from limited coverage observations. Since that report, the Kalman filter has undergone a statistical validation of its output error estimates against the statistics of the observed-minus-forecast assimilation residuals (Menard et al. 1997). This statistical validation study has enabled us to identified several deficiencies in the original algorithm and, hence, resulted in several modifications of the scheme.

A key feature of the Kalman filter is to evolve the estimation error covariance using a dynamical model, namely, the transport model of Lin and Rood (1996). Some deficiencies of the original algorithm were related to discretization of the covariance field. The evolution of error covariance in the continuum was studied first by Cohn (1993) and extended later to include the observation counterpart in Cohn (1997). The statistical validation conducted during this year has shown that very large discretization error arises

in the prediction of the error covariance, resulting in a significant loss of skill in the estimated analysis error variance. On the basis of Cohn (1993), a variance preserving scheme has been developed and successfully implemented. In addition, several other alternative schemes which have conservative properties of the correlation field are under development. The mismatch between the horizontal sampling of the continuum inherent in satellite observations and in the representation of the continuum by the transport model results in "error of representativeness", that needs to be accounted for during the assimilation. It was found that the representativeness error standard deviation for the CLAES methane with a 4x5 degree finite volume grid point model is about 10% of the signal, with a slightly lower value for the HALOE methane. The represenativiness error is larger than the instrument error for the gas and altitude considered (3.5% for the CLAES and 0.7% for the HALOE). Although, it is not yet clear how the representativeness error can be significantly reduced in practice so as to maximize the use of satellite observations in data assimilation, a preliminary study by Peter Lyster (personal communication) has indicated that for point measurements, the representativeness error only slowly decrease with increasing resolution. This, in turn, demands that very high resolution models be used in data assimilation schemes in order to take full advantage of point observations of constituents.

The statistical study has also helped us to reach the conclusion that forecast and representativeness errors are better described in terms of relative error rather than with an absolute error formalism. This finding corroborates the use of a multiplicative error assumption as is the case in the lognormal filter currently under development. The study has also been used to establish the statistically validated error variance of the Kalman filter analysis. When the CLAES methane observations are assimilated, a reduction of error variance of one order of magnitude is achieved over the observational error variance. A simpler assimilation scheme that has a fixed homogeneous isotropic correlation model give rises to a variance reduction not as large, about 2/3 of the observational error. The accuracy of the off-line transport alone was also established by using the statistics of the observation-minus-forecast residuals and knowing the observational error (that includes the representativeness error) established from the previous assimilation experiments. A relative standard deviation of about 12% at the 1100K isentrope and slowly increasing with time was established. All these error estimates were obtained under a two-dimensional isentropic approximation of the flow and of the assimilation scheme. Despite these limitations, the results are excellent compared with current standard in global data assimilation.

2.3.2 Ozone assimilation

Development of an operational three-dimensional ozone assimilation system is in progress at the DAO. The initial goal is to enable the DAO to provide high quality near-real time three-dimensional ozone fields as input to the EOS instrument teams. In the longer term we expect to use the data generated by the system also for process and trend studies. The assimilating model is the CTM developed jointly by the Atmospheric Chemistry and Dynamics Branch and the DAO at Goddard (Douglass et al., 1996; Lin and Rood, 1996). The model is driven by GEOS-DAS assimilation wind fields, and the input observations are TOMS total ozone and SBUV ozone profiles.

The analysis system itself is mainly designed along the lines of PSAS (Physical-space Statistical Analysis System; Cohn et al., 1997), the DAO meteorological analysis system. However, there are a couple of important differences with respect to the current implementation of that system. The ozone assimilation is being designed to work as a filter with continuous updates at every time step, rather than using a six-hourly forecast/analysis cycle as is common in assimilation for numerical weather prediction. The reason for this is that the ozone system is driven by satellite data obtained on a continuing basis, as opposed to meteorological systems that still rely extensively on conventional observations taken at the synoptic times. The method of continuous updates is computationally more efficient than the intermittent cycling, and it will also minimize phase errors due to the difference between the analysis time and the actual time of the observation. However, the ozone assimilations system is expected to be

more demanding than an intermittent system, as far as the validity of the forecast error covariance model is concerned. The forecast error covariance matrix formally contains N*(N+1)/2 independent elements, where N is the number of predicted variables - on the order of 10^6 for the ozone system, depending on resolution. This is both computationally and conceptually an unreasonable amount of information to generate and manipulate, and in current meteorological analysis systems the covariance is therefore modeled assuming isotropy, and often also homogeneity, of the forecast error. This greatly simplifies the problem, but the shape of the analysis increment then no longer depends on the actual state of the atmosphere. In particular, the increment added to the background field in order to obtain the analysis based on an isolated observation will be isotropic, a feature that is clearly unphysical, for instance, near a front.

In order to address this problem, a simple and inexpensive method for specifying the forecast error correlation directly in terms of the forecast field itself has recently been developed (Riishojgaard, 1997), and is currently being implemented in the ozone assimilation system. Fig. 2.3.2-1, which is based on data from Riishojgaard (op. cit.), shows an example of an analysis increment calculated from a single observation (at the asterisk) using this model (isolines), together with the difference between the true state and the forecast estimate (color shading) from a simple total ozone analysis experiment. It is clearly seen that the anisotropic model allows the increment to stretch out - as it should according to the background error field - in the E-W direction, while keeping it out of the area SW of the observation where the sign of the background error is the opposite of that at the observation location. For comparison, the increment due to a classic isotropic correlation model would be circular, and it would thus either be wrong over a large part of the domain, if the correlation length is assumed to be large, or it would be confined to a small neighborhood of the observation if the correlation length is assumed to be small. Straightforward generalizations of the model to non-linear three-dimensional problems have been proposed, but not yet tested.

2.4 Two dimensional models

2.4.1 Fixed Two Dimensional Model Studies

An important goal of our IDS investigation is to understand the changes which have occurred in the concentration of stratospheric ozone. To do this we use a variety of 2D, 3D, and trajectory models. Our understanding of the processes which control ozone is incorporated into models which can be used to make predictions of the changes of ozone which might be expected in the future. These models are usually termed "assessment" models. They always contain simplifying assumptions and are currently mostly 2D (latitude and altitude).

The GSFC fixed climatological 2D model is primarily funded through ACMAP, although there is partial EOS IDS support. The Goddard 2D assessment model has recently been reformulated with a new derivation of the meridional circulation and eddy coefficients (Fleming et al., in preparation, 1997). The new formulation is similar to that which has been used in the 2D coupled model developed under this proposal. The model dynamics are derived from an elliptic streamfunction which is based on a solution of the zonal momentum and energy equations along with the thermal wind equation. The temperatures, zonal-mean winds, and EP flux divergences are derived from data (17-year average of NMC data plus zonal mean winds in the equatorial region from HRDI on UARS). Thus, although the dynamical formulation is the same as the coupled model, dynamical feedbacks are not included and the model is constrained to the present atmosphere.

The 2D model develops a number of features which are qualitatively consistent with the behavior of stratospheric transport as derived from data analyses. In the southern hemisphere winter and early

spring, the model develops a clearly isolated vortex and midlatitude surf zone as exhibited by the methane mixing ratios shown in the accompanying figure. The equivalent behavior in the northern hemisphere does not occur. The model develops only the barest hint of the development of an isolated vortex. This is presumably because the derivation of the EP flux divergences has been done using the wave amplitudes derived from variations about a zonal mean. In the northern hemisphere, this means that near the vortex edge data from within and without the vortex is mixed together leading to enhanced mixing in the derivation.

Another feature which arises naturally in the formulation of this model is the partial isolation of the tropical region from the subtropics. A preliminary examination shows that the air rising in the tropics in the model has about 20-25% incorporated into the flow from the midlatitudes. This makes the model tropics somewhat more isolated than has been derived from data analyses. Analysis of the age of air derived from tracers such as CO2 in the model indicate that the oldest air in the model (age = time since entering through the tropical tropopause) is about one year younger than derivations from ER-2 CO2 data. This is possibly because the model does not recirculate enough of the midlatitude air through the tropics where it can be relofted to high altitudes. We are now at the point of examining specific deficiencies in the assessment models.

Another study was completed with the 2D model in which anthropogenically caused chlorine and bromine increases, solar cycle ultraviolet flux variations, and the changing sulfate aerosol abundance due to several volcanic eruptions were all included. The predictions of annually averaged total ozone between 65S and 65N over the 1960 to 2030 time period from that model simulation compared to measurements are shown in Figure 2.4.1-1 . The model captures much of the variability and downward trend in total ozone that is measured by the Total Ozone Mapping Spectrometer (TOMS) instruments, on Nimbus 7 and on Meteor 3, over the 1979 to 1994 time period.

The model simulations predict a decrease in total ozone of about 4% from 1979 to 1994 due to the chlorine and bromine increases. The changing sulfate aerosol abundances can also significantly affect total ozone with the Mt. Pinatubo eruption computed to cause a decrease in global ozone by about 3% in 1992. Solar ultraviolet flux variations cause increases and decreases in total ozone with computed changes of about 1% from solar maximum to minimum. Model predictions for the future indicate that total ozone should start to recover from its lowest levels by the late 1990's. Future measurements of ozone are crucial to help quantify the recovery process.

2.4.2 Interactive Two Dimensional Model Studies

Improvements to the interactive 2d model in 1997 include the attachment of the new chemistry package (used in the fixed 2D model) and revision of the tropospheric parameterization. We continue to collaborate with NRL on the development of the model.

Research with the interactive 2D model developed under this IDS has focused on studying the radiative effects of tropical subvisible cirrus clouds. These thin clouds have been observed at and just below the tropical tropopause by the DIAL lidar during the TOTE mission, as well as by in situ [Heymsfield, 1986] and satellite observations [Wang et al., 1994]. Our coupled model forms ice clouds not only in the polar stratosphere but also in the tropical troposphere just below the tropopause. In order to study the potential radiative impact of these clouds we have performed model runs in which the radiative heating due to these clouds is included. The ice cloud heating has been calculated using the method described in Rosenfield [1992].

The total mass of ice water predicted by the model is controlled by the model temperatures and water

vapor. Time-height contours of the model steady-state water vapor, shown in Fig. 2.4.2-1, show clearly the "tape recorder" signal and can be compared with Plate 1 of Mote et al. [1996]. Runs with ice particle sizes of 2, 6, and 10 microns were performed, with the 6 micron sized particles yielding scattering ratios in good agreement with those observed by the DIAL lidar during the TOTE mission. The increased diabatic heating of these clouds, 0.2-0.4 K/day, results in increasing temperatures and vertical velocity. The net result of the temperature increases of 2-5 K at and just below the tropical tropopause is an increase in the amount of water vapor reaching the stratosphere. Fig. 2.4.2-2 shows the water vapor computed at 51 hPa as a function of time of year for the case of no ice cloud heating and for the cases of ice cloud heating with various sized particles. For the 6 micron sized particles, 2 ppmv more water vapor reaches the lower stratosphere with the cloud heating than without. The impact of sedimentation was found to be negligible. Thus these results suggest that the presence of the subvisible cirrus clouds result in an increase in stratospheric water vapor, as opposed to acting as a dehydration mechanism, as proposed by Jensen et al. [1996]. These results are currently being written up for publication.

2.5 Sampling of high resolution data

During the previous reporting period, high-resolution (1 degree by 1 degree) global fields of potential vorticity were generated on the 560 K isentropic surface. Created using the Reverse Domain Filling (RDF) technique, these fields exhibit realistic fluid-dynamical features. They were produced for every six hours covering a span of 30 days.

These RDF data have now been used to estimate the kind of improvements HIRDLS high resolution sampling would achieve. Thirty days of satellite sounding locations were calculated, and the RDF fields were interpolated to those locations. The simulated measurements were then used to construct regularly gridded fields, using Delaunay triangulation and subsequent bilinear interpolation to the grid points. These data, gridded from the simulated observations, were then compared to the original RDF fields.

Four modes of satellite sampling were compared: The regular HIRDLS scanning pattern, the high-resolution HIRDLS scanning pattern, a hypothetical single-scan mode, and a hypothetical ultra-high-resolution scanning mode.

Figure 2.5-1 shows the original RDF field for 25 February, 1992, along with the simulated measurements for the single and regular scanning modes, as well as the gridded fields constructed from these measurements.

Statistical analyses are currently underway to quantify the degree of improvement in gridded fields provided by higher resolution scanning modes. In addition, it is planned to apply the Salby fast Fourier synoptic mapping technique to these simulated satellite data. From Fig. 2.5.1 it is not clear that the high resolution HIRDLS sampling makes a significant improvement in the retrieved fields.

2.6 TOMS data

We continue to analyze the data from TOMS instruments as part of this IDS. The ADEOS satellite failed in the spring of 1997, but EP TOMS is still operating. Total ozone observations from the Total Ozone Mapping Spectrometer (TOMS) instruments during March 1997 reveal an extensive region of low column amounts in the Arctic region centered near the north pole. Values were below 250 Dobson units (DU) for nearly a two week period during this period, and were correlated with the position of the northern lower stratospheric polar vortex. The March 1997 average total ozone column densities were more than 30% lower than the average of column densities observed during the 1979--1982 March period. A paper discussing these observations is in press in GRL [Newman et al., 1997].

2.7 Aircraft data analysis

2.7.1 Errors in ozone depletion due to small scale structure in chlorine

radicals

Aircraft observations of active chlorine show intense spatial variability on scales well below the resolution of global model grids. Edouard et al. [1996] proposed that the lack of resolution of these small scale features in numerical models produced an underestimate in ozone loss. In the work described below, the statistics of subgrid scale structure in active chlorine were computed from high resolution aircraft observations and were used to estimate the sensitivity of modeled ozone loss to the spatial resolution of the model grid.

A large fraction of the total ozone loss in the winter lower stratosphere occurs via the chlorine catalytic cycle, a process that is limited by the rate of ClO dimer formation. The nonlinearity of this process, together with the existence of small scale structure well below the spatial resolution of most model grids, mean that a model calculation of ozone loss will underestimate, to some extent, the actual ozone loss in the atmosphere. High resolution aircraft observations of ClO taken during the AASE II aircraft campaign were used to estimate the error in the ozone loss rate due to subgrid scale structure in the ClO field. Because the ozone loss rate depends quadratically on the concentration of ClO, which we denote below by , the low resolution loss rate for a model gridbox is proportional to $\langle\rangle^2$, while the actual loss rate is proportional to $\langle^2\rangle$. Here, <...> means an average over an LxL gridbox, which we approximate from the data by an average over the observations within data segments of varying lengths L. The difference between the high and low resolution loss rates is the local variance of , and we define a relative resolution error = var()/$\langle\rangle^2$.

Figures 2.7.1-1 shows the dependence of on for high (50 < L < 200 km), medium (250 < L< 450 km), and low (500 < L < 800 km), resolution grids. Each curve corresponds to the mean error <();L> in each range of grid scales, obtained by averaging over all those segments with lengths in that range. The dotted lines in each figure are approximate boundaries of the chemical edge of the vortex. Figure 2.7.1-1 shows small errors of only a few percent, and also shows little resolution dependence well inside the vortex, where <> is above 0.7 ppbv. Errors are largest at the vortex edge, where the resolution sensitivity is also largest. This can be seen more clearly in Figure 2.7.1-2 , which shows the dependence of the resolution error on gridscale L. We only consider three ranges of values of <>, corresponding to the three classes "out", "in" and "edge", as shown in Figure 2.7.1-1 . Each curve is the mean error <(L);>, obtained by averaging over data segments that have the same length and also have <> values within the same range. Overall, for typical grid scales in the range 100<L<500 km, increases approximately linearly from 5-35%.

2.7.2 TOTE/VOTE

We have done an analysis of the mixing processes within the lower polar stratosphere using the Tropical Ozone Transport Experiment/ Vortex Ozone Transport Experiment (TOTE/VOTE) ozone data. By looking at the inner vortex ozone changes and also looking at the amount of ozone outside the vortex it is clear that the diabatic cooling would build up ozone in the lower stratosphere. Using equal area trajectory analysis we have been able to estimate the mixing rate of lower ozone concentration mid-latitude air into the vortex. In the middle world (below 380K) this in mixing approaches 80%, but drops rapidly to 50% at higher altitudes. Using this mixing rate we can simulate the lower stratospheric ozone amounts quite well. These results were prepared for presentation at the AMS Middle Atmosphere Conference in Tacoma, 1997, and are being prepared for publication.

2.8 Tropospheric Chemistry

With co-funding from ACMAP, a modified-residual technique has been developed by Hudson and Thompson [1997] to retrieve half-monthly averaged tropical tropospheric column ozone from the TOMS radiances. This technique involves the extraction of a persistent wave-one pattern, with its maximum over the tropical Atlantic, as in Kim et al [1996]. Several improvements to the Kim et al. [1996] method have been incorporated in the modified-residual method. These include: (1) Fourier analysis of the wave pattern to set latitude limits for where the method is valid; (2) assumption that the wave-like pattern is in the troposphere; (3) normalization to the ozonesondes for 1991-92, the years for which the new method is complete. Because of the ozonesonde constraint, the derived troposphere ozone column amount can be compared to observations and imprecision assigned to the maps. The modified-residual method is now being applied to the 14-year Nimbus 7/TOMS record.

A variation of the modified residual method is used with real-time EP-TOMS gridded data to produce tropical tropospheric ozone maps as 1-day and 5-day averaged images (http:metosrv2.umd.edu/~tropo). A 5-day averaged map is shown in Figure 2.8-1 . Validating these maps is still underway. PEM-Tropics,(PEM = Pacific Exploratory Mission), a DC-8 mission, operated in the Central and Eastern Pacific in September-October 1996, and UV-DIAL and in-situ ozone data are available in a limited region within our tropical band. Ozone profiles are also available from ozonesondes launched at Samoa, Tahiti, and Easter Island. However the ozonesonde data fall a few degrees South of the region covered by the real-time maps. At Samoa, excursions of pollution ozone from biomass burning are evident on many days. These plumes do not always reach the 10S latitude. The major challenge in ascertaining whether or not Fig 2.8-1 displays an accurate ozone column is that there are no Atlantic or Indian Ocean tropical sondes for this period.

2.9 CRISTA Data

We have been comparing CRISTA and MLS O3 and temperature measurements for DOY (day number) 309 to DOY 315 when shuttle CRISTA data are available. Asynoptic zonal mean profile data (version B3 for CRISTA and level 3AT, version 4 for MLS) were used to study the differences between the raw data sets, while trajectory mapped synoptic data (using the GSFC adiabatic trajectory model) were used to quantify the superiority of CRISTA to study small-scale, rapidly varying features in the atmosphere.

Figures 2.9-1a and 2.9-1b show latitude-height contour plots for the zonal mean temperature measurements on DOY 310 from CRISTA and MLS. The CRISTA temperatures are low biased by about 2-6 degrees Kelvin over most of this domain. the MLS temperature uncertainty is quoted as being about 5 degrees Kelvin, and the CRISTA temperatures agree with MLS, given this uncertainty, over most of the domain. The spatial structures of the CRISTA and MLS measurements look similar except at southernmost latitudes where the CRISTA data show a temperature inversion persisting from DOY 309 to 315 at about 30 hPa. Figure 2.9-1c and 2.9-1d show latitude-height contour plots for CRISTA and MLS zonally-averaged O3 on DOY 311. The ozone maximum is located at about 10 hPa in both data sets. The vertical extent of the O3 maxima are consistently broader for the CRISTA measurements. The largest persistent disagreement between these two O3 data sets is between about 8 and 10 hPa at most latitudes where the CRISTA values for zonally-averaged O3 are larger by values ranging up to about 1 ppmv. This level of disagreement is larger than the quoted MLS accuracy in this region. For DOY 314, south of 28S, this discrepancy extends up to 5 hPa, with CRISTA O3 vmr being higher by as much as 1.5 ppmv (or about 30% of the MLS O3 vmr). It should be pointed out that MLS experienced antenna scanning problems during the time period of this study and screening of the MLS data was done to eliminate climatological data and data with an uncertainty larger than 50% (using the quality parameter).

To quantify the superior capability of CRISTA-type instruments (e. g., HIRDLS) to study small-scale, rapidly varying atmospheric features, we used the GSFC adiabatic trajectory model to obtain synoptic maps using both data sets. Each full day of CRISTA data yields about 5000 good O3 profiles while for MLS, there are only 1318 profiles. Two days of CRISTA data are normally enough to produce a good synoptic map while 4-5 days are needed for MLS data. Maps from both data sets show similar large-scale structures. Figure 2.9-1e shows the longitudinal O3 variation for DOY 311 at 26 degrees South on the 700 K potential temperature surface. Both CRISTA (solid line) and MLS (dashed line) maps were created using 5 days of data advected to midnight of DOY 310, treating O3 as a conserved species. The spatial structures are highly correlated (with a correlation coefficient of 0.75), but the CRISTA curve shows more small-scale variations. The differences in the zonal mean is very likely due to the height and temperature bias between the two data sets. Synoptic and asynoptic zonal means agree well, except in the tropics. For instance, the CRISTA synoptic zonal mean at 2.5S on DOY 311 is lower by as much as 1 ppmv compared to the asynoptic zonal mean calculated using all of the available primitive CRISTA data collected during DOY 311. (The same is also true for MLS.) We also compared the zonal mean of O3 latitudinal gradients using trajectory maps. On the 700K potential temperature surface, MLS gradients are generally higher than that for CRISTA in the tropics, being more than 30% higher in some cases. At latitudes south of 26S, CRISTA O3 gradients are generally higher.

3.0 References

Chipperfield, M. P., A. M. Lee, and J. A. Pyle, Model calculations of ozone depletion in the Arctic polar vortex for 1991/92 to 1994/95, Geophys. Res. Lett., 23, 559-562, 1996.

Cohn, S. E., Dynamics of short-term forecast error covariances. Mon. Wea. Rev., 121, 3123-3149, 1993

Cohn, S. E.: An introduction to estimation theory. J. Met. Soc. Japan, 75, 257-288, 1997.

Cohn, S. E., A. da Silva, J. Guo, M. Sienkiewicz, and D. Lamich Assessing the Effects of Data Selection with the DAO Physical-space Statistical Analysis System; (submitted to Mon. Wea. Rev.), 1997.

Douglass, A. R., C. J. Weaver, R. B. Rood, and L. Coy, A three-dimensional simulation of the ozone annual cycle using winds from a data assimilation system. J. Geophys. Res., 101, 1463-1474, 1996.

Douglass, A. R., R. B. Rood, S. R. Kawa, and D. J. Allen, A three dimensional simulation of the evolution of the middle latitude winter ozone in the middle stratosphere, J. Geophys. Res., 102, 19,217-19,232 ,1997.

Edouard, S., B. Legras, F. Lefevre and R. Eymard, The effect of small-scale inhomogeneities on ozone depletion in the Arctic., Nature, 384, 444-447, 1996.

Heymsfield, A.J., Ice particles observed in a cirriform cloud at -83 C and implications for polar stratospheric clouds, J. Atmos. Sci., 43, 851-855, 1986.

Jensen, E.J., et al., Dehydration of the upper troposphere and lower stratosphere by subvisible cirrus clouds near the tropical tropopause, Geophys. Res. Lett., 23, 825-828, 1996.

Hudson, R. D., and A. M. Thompson, Studies of the wave-one pattern in tropical total ozone: Implications for derivation of tropospheric ozone, J. Geophys. Res., manuscript in preparation, 1997.

Kim, J-H., R. D. Hudson and A. M. Thompson, A new method of deriving time-averaged tropospheric

column ozone over the tropics using total ozone mapping spectrometer (TOMS) radiances: Inter-comparison and analysis using TRACE-A data, J. Geophys. Res., 101, 24317-24330, 1996.

Lin, S.-J., and R. Rood, Multidimensional flux-form semi-Lagrangian transport schemes. Mon. Wea. Rev., 124, 2046-2070, 1996.

Lyster, P.M., S.E. Cohn, R. Menard, L.-P. Chang, S.-J. Lin, and R.G. Olsen, Parallel implementation of a Kalman filter for constituent data assimilation. Mon. Wea. Rev., 125, 1674-1686, 1977

Manney, G. L., et al., Arctic ozone depletion observed by UARS MLS during the 1994-1995 winter, Geophys. Res. Lett., 23, 85-88, 1996.

Manney, G. L., et al., 1994: Chemical depletion of ozone in the Arctic lower stratosphere during winter 1992-93, Nature, 370, 429-434, 1994.

Menard, R., L.-P. Chang, P.M. Lyster, and S.E. Cohn, 1997: Stratospheric assimilation of chemical tracer observations using a Kalman filter. Submitted to J. Geophys. Res., 1997.

Moody, J. et al. Observations of stratospheric ozone under a persistent cut-off low: AEROCE Spring 1996, Eos Trans. AGU, 78(17), Spring Meet. Suppl., S98, 1997.

Mote, P.W., An atmospheric tape recorder: The imprint of tropical tropopause temperatures on stratospheric water vapor, J. Geophys. Res., 101, 3989-4006, 1996.

Newman, P., J. Gleason, R. McPeters, R. Stolarski, Anomalously low ozone over the arctic, GRL, in press, 1997.

Riishojgaard, L. P., A direct way of specifying flow-dependent background error correlations for meteorological analysis systems, Tellus (in press), 1997.

Rosenfield, J.E., Radiative effects of polar stratospheric clouds during the Airborne Antarctic Ozone Experiment and the Airborne Arctic Stratospheric Expedition, J. Geophys. Res., 97, 7841-7858, 1992.

Sparling, L. C., A. R. Douglass and M. R. Schoeberl, An estimate of the effect of unresolved structure on modeled ozone loss from aircraft observations of ClO, Geophys. Res. Lett., 1997, submitted.

Wang, P.-H., et al., Tropical high cloud characteristics derived from SAGE II extinction measurements, Atmos. Res., 34, 58-83, 1994.

Weaver, C. J., A. R. Douglass, and D. B. Considine, A 5-year simulation of supersonic emission transport using a three-dimensional model J. Geophys. Res., 101, 20975-20984, 1996.

4.0 Figure Captions

Fig. 2.1.1-1. Distribution of parcels in a typical age-of-air calculation. Parcels are colored by age (in years). The background colors show the net diabatic heating rate in K/day. Solid line is zero heating. The thick line shows the tropopause.

Fig 2.1.1-2. Number of parcels verses altitude and a fit showing the scale height. Dotted line shows the atmospheric density decrease with altitude for comparison.

Fig. 2.1.1-3. The age-of-air using the Lagrangian method from UKMO winds (part a). The age-of-air using assimilation winds (part b).

Fig. 2.1.1-4. Age-of-air computed using the Goddard CTM and the assimilation winds (Courtesy of Susan Strahan).

Fig. 2.1.2-1. Time evolution of parcels after a uniform release from 20 to 60 N at 19km. The release region is simulates an effluent release by HSCT aircraft.

Fig. 2.2.1-1. Time evolution of modeled and observed chlorine constituents on the 500K surface for 1992.

Fig. 2.2.1-2. Same as Fig. 2.2.1-2 for 1997.

Fig. 2.3-1. Comparison of the 10 hPa potential vorticity for 16 Jan 1992 derived from four data assimilation systems: ERECS01_W91 is the newest GEOS-2 system, EPREFGGEC is the GOES-1 based stratospheric system, ETEST14 is an untuned version of GEOS-2, UKMO is the United Kingdom Meteorological Office stratospheric assimilation. Plots are from the equator to the north pole on a lambert equal area projection. 90W is at the bottom of each plot. Contour colors and intervals are the same in each plot. The horizontal resolution is 2.5 by 2 degrees (longitude by latitude) except for the UKMO which is 3.75 by 2.5 degrees. Note the smoother field generated by GEOS-2 (ERECS01_W91) compared to GEOS-1 (EPREFGGEC).

Fig. 2.3.2-1. Analysis increment for total ozone calculated from a single observation (asterisk) using the model (isolines), together with the difference between the true state and the forecast estimate of total ozone (color shading).

Fig. 2.4.1-1. Model calculation of past global changes and future projections for ozone change assuming that the provisions of the Montreal Protocol are followed. The calculation of past changes included the effect of increasing chlorine and bromine, solar cycle UV variations and volcanic aerosols. The annually averaged TOMS data are shown for comparison. The future changes include the effects of decreasing chlorine and bromine as well as solar-cycle changes.

Fig. 2.4.2-1. Steady state model computed water vapor (ppmv) averaged between 20S and 20N. The second year is a repeat of the first year.

Fig. 2.4.2-2. Model water vapor at 51 hPa, averaged between 20S and 20N, with and without ice cloud heating for different ice particle radii.

Fig. 2.5-1. This figure shows the results of using HIRDLS sampling to reconstruct high resolution data. The synthetic data are shown to the left. Using standard limb sounding sampling (single track sampling, middle top) the upper right data set is generated. Using the HIRDLS scanning pattern (lower middle) data set at the lower right is generated.

Fig. 2.7.1-1 Dependence of the mean error <()> on <> for high, medium and low resolution model grids, as defined in the text. The dotted lines are approximate boundaries of the chemical edge of the vortex.

Fig. 2.7.1-2 Dependence of the mean error <(L)> on grid scale L, for inside, outside or edge vortex gridboxes. Location with respect to the vortex is defined by the boundaries shown in Figure 1.

Fig. 2.8-1 5-day averaged tropical tropospheric ozone column from modified-residual method. Taken from real-time Earth Probe TOMS and posted at http://metosrv2.umd.edu/~tropo. Data can be obtained from hguo@atmos.umd.edu.

Fig. 2.9-1a and b DOY 310 zonally-averaged MLS and CRISTA temperature. The average is calculated using all the asynoptic profiled data collected during the day. Since a latitudinal interval of 3 degrees is used for each latitude circles calculated, the diurnal circle is well covered.

Fig. 2.9-1c and d Same as Figure 2.10-1a and b but for O3.

Fig. 2.9-1e Longitudinal synoptic O3 variation at 26S on 700K potential temperature at midnight of DOY311. The curves are taken from MLS and CRISTA synoptic maps produced using the GSFC adiabatic trajectory model. 5 days of data were used to produce the synoptic maps.

5.0 List of Publications

Bevilacqua, R.M., C.P. Aellig, D. J. Debrestian, M. D. Fromm, K. Hoppel, J. D. Lumpe, E. P. Shettle, J. S. Hornstein, C. E. Randall, D. Rusch, and J. Rosenfield, POAM II observations of the Antarctic ozone hole in 1994 and 1995, J. Geophys. Res., in press, 1997.

Considine, D.B., A.E. Dessler, J.E. Rosenfield, P.E. Meade, M.R. Schoeberl, A.E. Roche, and J.W. Waters, Interhemispheric asymmetry in the 1 mbar O3 trend: An analysis using an interactive zonal mean model and UARS data, J. Geophys. Res., in press, 1997.

Menard, R., L.-P. Chang, P.M. Lyster, and S.E. Cohn, 1997: Stratospheric assimilation of chemical tracer observations using a Kalman filter., submitted to J. Geophys. Res, 1997.

Newman, P.A. and J.E. Rosenfield, Stratospheric thermal damping times, Geophys. Res. Lett., 24, 433-436, 1997.

Newman, P., J. Gleason, R. McPeters, R. Stolarski, Anomalously low ozone over the arctic, GRL, in press, 1997.

Rosenfield, J.E., D.B. Considine, P.E. Meade, J.T. Bacmeister, C.H. Jackman, and M.R. Schoeberl, Stratospheric effects of the Mt. Pinatubo aerosol studied with a coupled two-dimensional model, J. Geophys. Res., 102, 3649-3670, 1997.

Rosenfield, J.E., et al., The impact of subvisible cirrus clouds near the tropical tropopause on stratospheric water vapor, submitted to JGR, 1997

Schoeberl, M. R., C. H. Jackman, and J. E. Rosenfield, A Lagrangian estimate of aircraft effluent lifetime, submitted to JGR, 1997.

Sparling, L. C., A. R. Douglass and M. R. Schoeberl, An estimate of the effect of unresolved structure on modeled ozone loss from aircraft observations of ClO, submitted Geophys. Res. Lett., 1997.

6.0 Automailer Usage

The automailer is a free service to atmospheric scientists. The automailer allows the downloading of

stratospheric meteorological products such as winds, temperatures, potential vorticity, and the generation of maps as post script files. The automailer can also be used to run the GSFC trajectory model (developed and maintained under this IDS). Calculations are run on a dedicated Silicon Graphics workstation supported by this IDS. The usage statistics for 1996 are given below. There were about 2000 more accesses in this period than in the previous annual period.

Automailer usage covering 1996-01-01 to 1996-12-31

USER ACCESSES

TOTALS: 103 users, 7083 accesses

FUNCTION	ACCESSES
curtain	219
metmaps	143
metprofile	2582
plot_met	1965
trajectory	2174